Quasi-TEM Description of MMIC Coplanar Lines Including Conductor-Loss Effects

Wolfgang Heinrich

Abstract—**A quasi-TEM model of MMIC coplanar structures is presented. The elements of the distributed equivalent circuit are calculated by closed-form approximations and hence can easily be implemented into CAD packages. The effects of non-ideal conductors are included as well as substrate loss and finite metallization thickness. The description holds for the entire quasi-TEM range, i.e., for typical MMIC geometries from DC to mm-wave frequencies. Validity of the model was checked by comparison to full-wave results. The errors for the effective dielectric constant and the characteristic impedance range below 5%, for the attenuation typical values of 5···10% are found (maximum: 20%).**

I. Introduction

IN MODERN monolithic microwave integrated circuits (MMIC's) more and more the coplanar waveguide (CPW) is used as transmission-line element [1]. The description of such miniaturized CPW structures, therefore, constitutes an essential part of any MMIC design tool. Fig. 1 shows the CPW geometry under consideration and the parameter definitions. Previous rigorous analyses [2]–[4] indicate clearly that any reliable modelling approach must take into account both finite metallization thickness and non-ideal conductors. On the other hand, the quasi-TEM condition holds well, even in the mm-wave frequency range. Hence an equivalent-circuit model as illustrated by Fig. 2 can be applied (note that the elements are defined per length, i.e., their unit reads 1/m). Such a description offers advantages because the elements can be derived separately and it fits well into common network analysis environment. For microstrip, several authors [5]–[7] have published corresponding work but their descriptions employ numerically expensive methods and hence they offer only a limited potential regarding most practical applications.

Extracting the elements R, L, C and G from the corresponding full-wave results [3], one finds that the variation of C and G/ω with frequency remains negligible whereas resistance R and inductance L exhibit considerable frequency dependence (see also [8]). The latter behavior can be explained by the change in CPW current-density distribution when increasing the frequency from DC to the skin-effect range.

For high frequencies, current penetration into the conductors is shallow and, consequently, R can be derived by a perturbation approach. Also, the internal and external parts

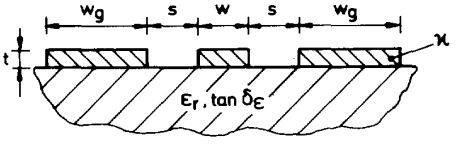

Fig. 1. The CPW cross section ($\mu = \mu_0, \varepsilon = \varepsilon_0$ except for substrate, κ denotes the conductivity of the metallization).

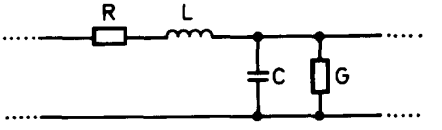

Fig. 2. The distributed equivalent-circuit model (all elements are defined per length).

of the inductance L_i and L_e may be separated with L_e being approximately frequency independent and identical to the value $L_{e\infty}$ for ideal conductors. Furthermore, the internal reactance ωL_i equals the resistance R. For skin depth values δ larger than about three times the metallization thickness t one faces a more complicated situation. Then, the current distribution changes significantly and also the external inductance becomes frequency dependent [9]. Regarding MMIC structures, however, also that range must be covered by the model.

To determine the four elements R, L, G, and C we proceed as follows:

1. An analytical approximation for the capacitance is derived assuming an arbitrary value of ε_r. This yields the line capacitance C and, applying the case $\varepsilon_r = 1$, the external inductance $L_{e\infty}$ according to the well-known quasi-TEM relation.
2. Once $L_{e\infty}$ is known R and ωL_i within the skin-effect range can be obtained by using the incremental inductance rule [10]. Since $L_{e\infty}$ is available in closed form also the derivatives with respect to the conductor dimensions can be calculated analytically.
3. For frequencies with $\delta \geq t/3$, additional investigations are necessary to develop a suitable approximation for the resistance that covers the complete frequency band. Similarly, the inductance must be treated to account for the frequency dependence of both external and internal parts.

Finally, the results calculated by our model are compared with full-wave mode-matching calculations [3] to validate the

Manuscript received January 30, 1992; revised April 30, 1992. This work was supported by the Deutsche Forschungsgemeinschaft (DFG).

The author is with the Institut für Hochfrequenztechnik, Technische Hochschule Darmstadt Merckstrasse 25, D-6100 Darmstadt, Germany.

IEEE Log Number 9204031.

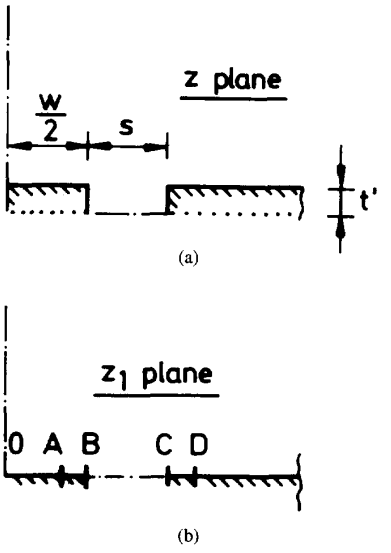

Fig. 3. The geometry used for calculation of the capacitance (z plane) and the structure after mapping into the z_1 plane (chain-dotted and solid lines denote magnetic and electric walls, respectively).

simplified approach and to evaluate its accuracy. One should emphasize that the approximative formulas are developed using physical arguments. Pure curve-fitting procedures are introduced only in the third step to describe the behavior within certain transition intervals.

In order to enhance clearness of presentation the following sections focus on the derivation of the approximations and the principal behavior of the line elements. Most of the formulas are not included there but summarized in the Appendix.

II. Calculation of the Capacitance

If one neglects the influence of the backside metallization and assumes the ground metallizations to extend to infinity the problem reduces to that illustrated by Fig. 3(a). Only one quarter of the cross section is considered, which corresponds to a capacitance $C_q = C/4$. For the case $\varepsilon_r = 1$ the thickness t' is equal to half the metallization thickness t defined in Fig. 1, for $\varepsilon_r > 1$ a magnetic wall can be placed at the substrate surface with good approximation. Then one has $t' = t$ for the upper half plane and $t' = 0$ for the lower one.

On principle, the capacitance C_q can be derived for arbitrary values of t' by means of a Schwartz-Christoffel conformal-mapping procedure. First, the complex z plane is transformed into the z_1 plane of Fig. 3. In the z_1 plane, one has again a CPW geometry but of zero thickness. Thus its capacitance can be determined easily [11]. The problem is that the coefficients B and C defining the resulting slot width are defined in the z_1 plane and not in the original one. Therefore, a nonlinear system of equations has to be solved that, additionally, contains integrals for which no analytical solutions exist. This approach is not suitable for the desired CAD purposes.

Owyang and Wu [12] applied a perturbation method to obtain a first-order approach for small but finite values of t'. Unfortunately, their mathematical derivation contains an inconsistency, which leads to erroneous results, e.g., a simple '$\ln t$' dependence of R. Revising their derivation, however, one obtains a reliable approximation for C_q in the case $t' \to 0$.

But such an approach is not sufficient regarding the CPW structures of interest since t' may exceed the limitations given by the first-order assumption. Hence, additional considerations are mandatory. One knows, for instance, the limit for large values of t'. Then, when increasing thickness t', the capacitance increment is simply that of a parallel-plate geometry, i.e., it holds $\partial C_q/\partial t' = \varepsilon_0/s$. It turns out that this limit is reached with good accuracy already for $t' = s/2$. What is left is the intermediate range between the first-order expression in t' and the point $t' = s/2$. In order to obtain a realistic approximation for that domain we introduce additional second-order terms for the interval $t' \leq s/2$. Their coefficients are determined such that the transition at $t' = s/2$ becomes continuous up to the second derivative. In this way, one achieves a smooth curve behavior between the two limits in t', which closely follows the exact results. Finally, the effect of finite ground planes is accounted for by modifying the term independent of t' according to [13].

The resulting formula for the capacitance reads $C_q(t') = \varepsilon \cdot F(t')$ with $F(t')$ being the function given in (1), shown at the bottom of the page. Here $K(k)$ and $K'(k)$ denote complete elliptic integrals of the first kind, for the coefficients k_i and p_{ci} please refer to (14) and (16) in Appendices A.1 and A.2. One should note already at this point that the *derivative* of C_q with respect to t' becomes infinite at $t' = 0$ due to the term $t' \cdot \ln t'$.

Using (1) one has for the total line capacitance C and the conductance G caused by the substrate dielectric-loss tangent:

$$\begin{aligned} C &= 2\varepsilon_0 \cdot (F_{\text{up}} + \varepsilon_r \cdot F_{\text{low}}) \\ G &= 2\omega\varepsilon_0\varepsilon_r \cdot \tan\delta_\varepsilon \cdot F_{\text{low}} \end{aligned} \tag{2}$$

with

$$\begin{aligned} F_{\text{up}} &= F(t' = t) \\ F_{\text{low}} &= F(t' = 0) = \frac{K(k_1)}{K'(k_1)} \cdot \end{aligned}$$

$$F(t') = \begin{cases} \dfrac{K(k_1)}{K'(k_1)} + p_{c0} \cdot \left\{ \dfrac{t'}{s} \cdot \left(p_{c1} - \ln \dfrac{2t'}{s} \right) + \left(\dfrac{t'}{s} \right)^2 \cdot \left(1 - \dfrac{3}{2} p_{c2} + p_{c2} \cdot \ln \dfrac{2t'}{s} \right) \right\} & \text{for } t' \leq \dfrac{s}{2} \\ \dfrac{K(k_1)}{K'(k_1)} + \dfrac{p_{c0}}{8} \cdot (p_{c2} + 2) + \dfrac{t'}{s} & \text{otherwise} \end{cases} \tag{1}$$

Similarly, the external inductance for ideal conductors $L_{e\infty}$ can be obtained from the capacitance for $\varepsilon_r = 1$ (we assume $\mu = \mu_0$ throughout the paper):

$$L_{e\infty} = \frac{\mu_0}{4F_0} \tag{3}$$

with

$$F_0 = F(t' = t/2)$$

The approximations used in the derivation of (1) introduce less than 1% error in capacitance and $L_{e\infty}$ for realistic dimensions.

III. The Skin-Effect Values of R and L_i

In the skin-effect region, i.e., if skin depth δ is small enough compared with metallization thickness t, a perturbation approach can be applied to determine line resistance R and internal inductance L_i. Because the inductance $L_{e\infty}$ is given in closed form Wheeler's incremental inductance rule [10] represents the best choice in our case. One only needs to calculate the inductance increments when recessing the conductors, which is a tedious but straightforward procedure.

The future treatment requires to distinguish between the ohmic losses on center and ground conductor. Therefore, the expression of (1) must be modified to include different values for the thicknesses of the two conductors. Again, the result can be given in an analytic form:

$$\begin{aligned} R_c|_{SE} &= \sqrt{\frac{\omega\mu_0}{2\kappa}} \cdot \frac{F_L^{(c)}}{4F_0^2} \\ R_g|_{SE} &= \sqrt{\frac{\omega\mu_0}{2\kappa}} \cdot \frac{F_L^{(g)}}{4F_0^2} \\ L_i|_{SE} &= \sqrt{\frac{\mu_0}{2\omega\kappa}} \cdot \frac{F_L^{(c)} + F_L^{(g)}}{4F_0^2} \end{aligned} \tag{4}$$

where $R = R_c + R_g$. The indices c and g refer to the center and ground conductors, respectively. 'SE' denotes the skin-effect region (for $F_L^{(c)}$ and $F_L^{(g)}$ please see (17) and (18) in Appendix A.3).

IV. The Line Resistance R

Fig. 4 shows the frequency dependence of the total resistance, i.e., the sum of the resistances R_c and R_g of center and ground conductors, respectively. Both in the high-frequency and the low-frequency limit one observes well-known characteristics. For frequencies f beyond about 20 GHz the skin-effect range appears with $R \sim \sqrt{f}$. For $f \to 0$, on the other hand, R approaches the DC value (f_{ci} and f_{gi} denote the corresponding transition frequencies for center and ground conductor, respectively). The DC resistance can be derived easily, (4) provides the skin-effect limit.

Between these two ranges, however, the behavior differs substantially from that of the classical skin-depth theory, which is based on simple one-dimensional considerations. The reason is that we are dealing here with a true two-dimensional current distribution (see [9]). This represents an essential extension compared to the magnetic-wall model of the microstrip, for instance. As a result, the so-called phenomenological loss

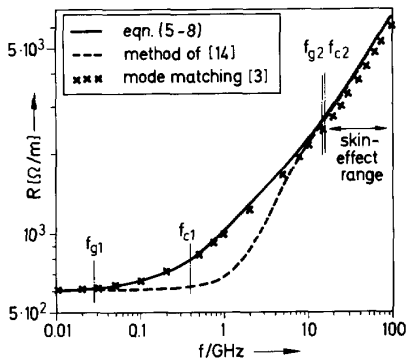

Fig. 4. CPW total line resistance R as a function of frequency f. Comparison of mode-matching results (symbols) with "phenomenological loss equivalence method" [14] (dashed) and this work (solid). The transition frequencies ω_{ci} and ω_{gi} according to (8) are indicated by the chain-dotted bars. (CPW structure with $w = 40\,\mu m, s = 5\,\mu m, t = 1.5\,\mu m, w_g = 200\,\mu m, \kappa = 3 \cdot 10^7$ S/m, $\varepsilon_r = 12.9$, for parameter definition see Fig. 1).

equivalence method [14] fails to predict the intermediate range (see dashed curve in Fig. 4).

Consequently, we employ a segmentation approach in developing an approximate expression for the resistances R_c and R_g of center and ground metallization: The curves $R(\omega)$ are defined piecewise within the three intervals. Regarding the intermediate range between DC and skin-effect approximation, a curve behavior linear in the log-log scale is assumed. As can be seen from Fig. 4, this setting closely fits the full-wave results. Finally, smoothing terms $a_i^{c,g}$ are included such that both R and $\partial R/\partial\omega$ remain continuous at the boundaries of the different intervals.

Equations (5)–(8) present the results for the total line resistance R:

$$R = R_c + R_g \tag{5}$$

(for R_c and R_g see (6) and (7) on the following page), where

$$\begin{aligned} R_{c0} &= \frac{1}{\kappa w t} \\ R_{c1} &= \sqrt{\frac{\omega_{c2}\mu_0}{2\kappa}} \cdot \frac{F_L^{(c)}}{4F_0^2} \\ R_{g0} &= \frac{1}{2\kappa w_g t} \\ R_{g1} &= \sqrt{\frac{\omega_{g2}\mu_0}{2\kappa}} \cdot \frac{F_L^{(g)}}{4F_0^2} \end{aligned}$$

$$\begin{aligned} \omega_{c1} &= \sqrt{2} \cdot \frac{4}{\mu_0\kappa t w} \\ \omega_{c2} &= \frac{8}{\mu_0\kappa} \cdot \left(\frac{w+t}{wt}\right)^2 \\ \omega_{g1} &= \frac{2}{\mu_0\kappa t w_g} \\ \omega_{g2} &= \frac{2}{\mu_0\kappa} \cdot \left(\frac{2w_g + t}{w_g t}\right)^2 \end{aligned} \tag{8}$$

$$\nu_c = \frac{\ln\left(\frac{R_{c0}}{R_{c1}}\right)}{\ln\left(\frac{\omega_{c1}}{\omega_{c2}}\right)}$$

$$\nu_g = \frac{\ln\left(\frac{R_{g0}}{R_{g1}}\right)}{\ln\left(\frac{\omega_{g1}}{\omega_{g2}}\right)}$$

(for $a_i^{(c)}$ and $a_i^{(g)}$, $(i = 1 \cdots 4)$, see (21) in Appendix A.5).

One should mention that the skin-effect limit of (5)–(8) deviates from the full-wave results by a certain extent. The greater the influence of the metallization edges, i.e., the smaller the ratio s/w, the more pronounced that effect becomes. It can be attributed to a principal error of the perturbation approach. The assumption of a constant skin depth δ fails in describing the realistic field behavior at metallic edges and overestimates the losses.

V. The Line Inductance L

The frequency behavior of L is plotted in Fig. 5. One observes a distinct frequency dependence. Also, L cannot be described simply by the inductance $L_{e\infty}$ found in the case of ideally conducting metallizations.

In the skin-effect realm, that is for $f \geq f_{L2}$, we find the well-known characteristics: L separates into an external part equal to $L_{e\infty}$ and an internal part L_i, which is related to the resistance and follows a $1/\sqrt{f}$ rule (see (4)). This situation changes when reducing frequency f below f_{L2}. Then inductance increases steeply. Only at very low frequencies, the curve saturates again towards its DC limit L_{DC0}. The value L_{DC0} can be derived analytically applying common magnetostatic theory. Equations (19) and (20) in Appendix A.4 provide the result. In our case, L_{DC0} assumes about double the value of $L_{e\infty}$. The substantial increase originates mainly from the *external* inductance L_e. The contribution of the internal part L_i remains in the order of 10% over the entire frequency range. This finding corresponds to results on two-wire configurations [15] but is in contrast to the common microstrip case where L_e is approximately constant with frequency and only L_i causes dispersion.

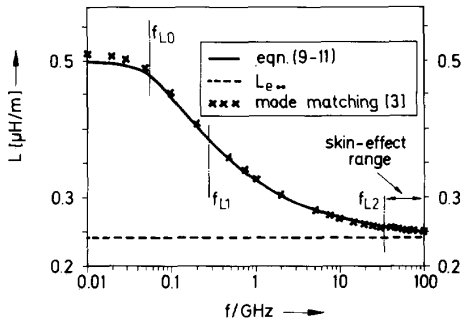

Fig. 5. CPW total line inductance L as a function of frequency f: mode-matching results (symbols), (9)–(11) (solid), and external inductance for ideal conductors $L_{e\infty}$ (dotted). The transition frequencies ω_{Li} according to (11) are indicated by the chain-dotted bars. For CPW data see Fig. 4.

The procedure to develop an approximative formula for L resembles that used for the resistance R. The curve is synthesized piecewise subdividing the entire frequency range into four intervals defined by the transition frequencies f_{Li} (see Fig. 5). f_{L2} denotes the lower limit of the skin-effect range and corresponds to the condition $t = 3\delta$. f_{L1} specifies the frequency where the current distribution in the center conductor becomes uniform. f_{L0} is associated with the frequency at which also the ground-metallization current approximates the DC distribution. After all, smoothing terms with coefficients

$$R_c = \begin{cases} R_{c0} \cdot \left[1 + a_1^{(c)} \cdot \left(\frac{\omega}{\omega_{c1}}\right)^2\right] & \text{for } \omega \leq \omega_{c1} \\ R_{c1} \cdot \left(\frac{\omega}{\omega_{c2}}\right)^{\nu_c} \cdot \left[1 + a_2^{(c)} \cdot \left(\frac{\omega_{c1}}{\omega}\right)^2 + a_3^{(c)} \cdot \left(\frac{\omega}{\omega_{c2}}\right)^2\right] & \text{for } \omega_{c1} \leq \omega \leq \omega_{c2} \\ \sqrt{\frac{\omega\mu_0}{2\kappa}} \cdot \frac{F_L^{(c)}}{4F_0^2} \cdot \left[1 + a_4^{(c)} \cdot \left(\frac{\omega_{c2}}{\omega}\right)^2\right] & \text{for } \omega \geq \omega_{c2} \end{cases} \tag{6}$$

$$R_g = \begin{cases} R_{g0} \cdot \left[1 + a_1^{(g)} \cdot \left(\frac{\omega}{\omega_{g1}}\right)^2\right] & \text{for } \omega \leq \omega_{g1} \\ R_{g1} \cdot \left(\frac{\omega}{\omega_{g2}}\right)^{\nu_g} \cdot \left[1 + a_2^{(g)} \cdot \left(\frac{\omega_{g1}}{\omega}\right)^2 + a_3^{(g)} \cdot \left(\frac{\omega}{\omega_{g2}}\right)^2\right] & \text{for } \omega_{g1} \leq \omega \leq \omega_{g2} \\ \sqrt{\frac{\omega\mu_0}{2\kappa}} \cdot \frac{F_L^{(g)}}{4F_0^2} \cdot \left[1 + a_4^{(g)} \cdot \left(\frac{\omega_{g2}}{\omega}\right)^2\right] & \text{for } \omega \geq \omega_{g2} \end{cases} \tag{7}$$

$a_i^{(L)}$ are introduced that ensure L and its first derivative to behave continuous at the transition frequencies. One obtains expression (9), shown at the bottom of the page, where

$$\begin{aligned} L_{\mathrm{DC0}} &= L_{\mathrm{DC}}(w, w_g) \\ L_{z1} &= L_{\mathrm{DC}}\left(w, \frac{3}{2}w\right) - \frac{\mu_0}{4} \cdot \frac{1}{F_1} \end{aligned} \tag{10}$$

with

$$\begin{aligned} F_1 &= F_0 + \frac{K(k_2)}{K'(k_2)} - \frac{K(k_1)}{K'(k_1)} \\ L_{z2} &= \sqrt{\frac{\mu_0}{2\omega_{L2}\kappa}} \cdot \frac{F_L^{(c)} + F_L^{(g)}}{4F_0^2} \end{aligned}$$

and

$$\begin{aligned} \omega_{L0} &= \frac{4}{\mu_0 \kappa t w_g} \\ \omega_{L1} &= \frac{4}{\mu_0 \kappa t w} \\ \omega_{L2} &= \frac{18}{\mu_0 \kappa t^2} \end{aligned} \tag{11}$$

$$\begin{aligned} \nu_{z1} &= \frac{\ln\left(\dfrac{L_{\mathrm{DC0}} - L_{e\infty}}{L_{z1}}\right)}{\ln\left(\dfrac{\omega_{L0}}{\omega_{L1}}\right)} \\ \nu_{z2} &= \frac{\ln\left(\dfrac{L_{z1}}{L_{z2}}\right)}{\ln\left(\dfrac{\omega_{L1}}{\omega_{L2}}\right)} \end{aligned}$$

L_{DC} denotes the DC inductance function given by (19) in Appendix A.4, $L_{e\infty}$ the external inductance for ideal conductors (3)), F_0 also refers to (3), and for $a_i^{(L)}, i = 0 \cdots 5$, see (22) in Appendix A.6.

In Fig. 5 one observes slight discrepancies for $f \to 0$ between the mode-matching analysis and (9)–(11). The reason is that for the mode-matching approach magnetic side walls are assumed whereas in the structure of Fig. 1 the substrate extends to infinity. Note that (9)–(11) give the exact DC value for the line geometry of Fig. 1.

VI. Restrictions and Errors

Our model employs a quasi-TEM approach. Thus, frequency must not exceed the value where non-TEM effects deteriorate accuracy considerably. This can be avoided if the actual wavelength does not fall short of about 10 times the characteristic waveguide dimensions, i.e., if $\lambda_0/(10\sqrt{\varepsilon_r}) \geq w + 2s$ holds. The formulas presented refer to a CPW structure of infinite substrate thickness without backside metallization. Hence, regarding the typical MMIC geometry a lower bound on substrate thickness h_s exist. Allowing for 1% deviation of the propagation quantities relations 12 specify the range of validity:

$$\begin{aligned} f &\leq \frac{1}{10} \cdot \frac{1}{\sqrt{\mu_0 \varepsilon_0 \varepsilon_r}} \cdot \frac{1}{w + 2s} \\ h_s &\geq 2 \cdot (w + 2s). \end{aligned} \tag{12}$$

Furthermore, the segmentation procedures used for L and R require that

$$w_g > w \qquad \text{and} \qquad t < \frac{9}{2}w \tag{13}$$

hold, which is fulfilled for the structures of practical interest.

Given the line elements R, L, C, and G the propagation quantities $\varepsilon_{\mathrm{reff}} = (\beta/\beta_0)^2, \alpha$, and the complex characteristic impedance Z can be easily derived. We checked the accuracy of the new model by comparing those quantities to the corresponding full-wave results of the mode-matching analysis [3]. Employing a variety of realistic MMIC coplanar structures the errors $|\Delta\varepsilon_{\mathrm{reff}}/\varepsilon_{\mathrm{reff}}|$ and $|\Delta Z/Z|$ can be estimated to be less than 3% (i.e., $|\Delta\beta/\beta| < 1.5\%$). For the attenuation α, the error bound is larger (20%). Generally, the errors decrease with growing impedance. Considering 50 Ω- geometries, for instance, the accuracy of α is better than 5%. Presenting plots of the propagation behavior would exceed the limitations of this paper. The interested reader is referred to [16].

Among the error sources mainly the resistance R has to be mentioned. For small slot widths the perturbation approach for the skin-effect region overestimates R by an order of 10%. Therefore, when developing a further improved description first (5)–(8) should be revised.

$$L = \begin{cases} L_{\mathrm{DC0}} \cdot \left[1 + a_0^{(L)} \cdot \left(\dfrac{\omega}{\omega_{L0}}\right)^2\right] & \text{for } \omega \leq \omega_{L0} \\ L_{e\infty} + L_{z1} \cdot \left(\dfrac{\omega}{\omega_{L1}}\right)^{\nu_{z1}} \cdot \left[1 + a_1^{(L)} \cdot \left(\dfrac{\omega_{L0}}{\omega}\right)^2 + a_2^{(L)} \cdot \left(\dfrac{\omega}{\omega_{L1}}\right)^2\right] & \text{for } \omega_{L0} \leq \omega \leq \omega_{L1} \\ L_{e\infty} + L_{z2} \cdot \left(\dfrac{\omega}{\omega_{L2}}\right)^{\nu_{z2}} \cdot \left[1 + a_3^{(L)} \cdot \left(\dfrac{\omega_{L1}}{\omega}\right)^2 + a_4^{(L)} \cdot \left(\dfrac{\omega}{\omega_{L2}}\right)\right] & \text{for } \omega_{L1} \leq \omega \leq \omega_{L2} \\ L_{e\infty} + \sqrt{\dfrac{\mu_0}{2\omega\kappa}} \cdot \dfrac{F_L^{(c)} + F_L^{(g)}}{4F_0^2} \cdot \left[1 + a_5^{(c)} \cdot \left(\dfrac{\omega_{L2}}{\omega}\right)\right] & \text{for } \omega \geq \omega_{L2} \end{cases} \tag{9}$$

VII. Conclusions

Evaluating the results of this paper the following conclusions can be drawn with regard to analysis and design of miniaturized MMIC CPW's:

- The quasi-TEM approach yields sufficient accuracy up to mm-wave frequencies.
- Both finite thickness of the metallizations and their non-ideal conductivity have to be accounted for.
- The field characteristics of the CPW are two-dimensional on principle. Thus approximations for strip resistance R and inductance L adopted from one-dimensional considerations fail to predict important effects. As a further consequence, the external inductance becomes frequency dependent to a substantial amount.
- The formulas given in this paper provide a very efficient formulation. Compared to equivalent full-wave analyses the numerical expenses are reduced drastically to the PC format. The resulting errors appear to match well with the practical requirements. The description consists of mathematical expressions that are lengthy but of closed-form. Therefore, it is particularly suited for implementation into CAD packages and related applications.
- The validity range of the model extends down to DC, which is of special interest regarding digital circuits.

VIII. Appendix A
The Parameters and Abbreviations Used

A.1 The Elliptic Integrals K and E and their Modulus k_i

$$K(k) - \text{complete elliptic integral of 1st kind}$$
$$E(k) - \text{complete elliptic integral of 2nd kind}$$
$$K'(k) = K(\sqrt{1-k^2})$$
$$E'(k) = E(\sqrt{1-k^2})$$

$$k_0 = \frac{w}{w+2s}$$
$$k_1 = k_0 \cdot \sqrt{\frac{1-\left(\frac{w+2s}{w+2s+2w_g}\right)^2}{1-\left(\frac{w}{w+2s+2w_g}\right)^2}} \tag{14}$$
$$k_2 = k_0 \cdot \sqrt{\frac{1-\left(\frac{w+2s}{4w+2s}\right)^2}{1-\left(\frac{w}{4w+2s}\right)^2}}.$$

Subroutines providing the elliptic integrals $E(k)$ and $K(k)$ are available on many computer platforms. Otherwise, efficient algorithms and approximate formulas can be found in the mathematical literature (e.g., [17], [18]).

A.2 The Coefficients p_{ci} and the Geometrical Parameters a, b, and t_H

$$a = \frac{w}{2}$$
$$b = \frac{w}{2} + s \tag{15}$$
$$t_H = \frac{t}{2}$$

$$p_{c0} = \frac{b}{2a}\frac{1}{(K'(k_0))^2}$$
$$p_{c1} = 1 + \ln\left(\frac{8\pi a}{a+b}\right) + \frac{a}{a+b}\ln\frac{b}{a}$$
$$p_{c2} = p_{c1} - 2\frac{a}{b}\cdot(K'(k_0))^2$$
$$p_{c3} = \frac{2b^2}{a(b+a)}\cdot\frac{E'(k_0)}{K'(k_0)} \tag{16}$$
$$p_{c4} = \frac{b-a}{b+a}\cdot\left[\ln\left(\frac{8\pi a}{a+b}\right) + \frac{a}{b}\right]$$
$$p_{c5} = \frac{b-a}{b+a}\ln 3$$
$$p_{c6} = \frac{b-a}{b+a}\ln\left(\frac{24\pi b(a+b)}{(b-a)^2}\right) - \frac{b}{b+a}\ln\frac{b}{a}.$$

A.3 The Quantities $F_L^{(c)}$ and $F_L^{(g)}$

Applying the incremental inductance rule one obtains for the center conductor (17) and correspondingly for the ground metallization (18) (see following page).

A.4 The DC Inductance L_{DC}

The DC inductance for the CPW of Fig. 1 (finite conductor thickness t, center strip width w_1, slot width s, ground metallization width w_2, infinite substrate) can be derived analytically:

$$\begin{aligned} L_{\mathrm{DC}}(w_1,w_2) = \frac{\mu_0}{8\pi}\cdot\Bigg\{ & \frac{4}{w_1^2}\cdot g_L(w_1) \\ & + \frac{1}{w_2^2}\cdot[g_L(w_1+2s) \\ & \quad + g_L(w_1+2w_2+2s) + 2g_L(w_2) \\ & \quad - 2g_L(w_1+w_2+2s)] \\ & - \frac{4}{w_1 w_2}\cdot[g_L(w_1+w_2+s) \\ & \quad - g_L(w_1+s) + g_L(s) - g_L(w_2+s)]\Bigg\} \end{aligned} \tag{19}$$

with the function $g_L(x)$ according to (20):

$$\begin{aligned} g_L(x) = & \left(\frac{1}{12}t^2 - \frac{1}{2}x^2\right)\cdot\ln\left\{1+\left(\frac{x}{t}\right)^2\right\} \\ & + \frac{1}{12}\frac{x^4}{t^2}\cdot\ln\left\{1+\left(\frac{t}{x}\right)^2\right\} \\ & - \frac{2}{3}\cdot x\cdot t\cdot\left\{\arctan\frac{x}{t} + \left(\frac{x}{t}\right)^2\cdot\arctan\frac{t}{x}\right\} \end{aligned} \tag{20}$$

A.5 The Coefficients $a_i^{(c)}$ and $a_i^{(g)}$

The coefficients $a_i^{(c)}$ and $a_i^{(g)}$ $(i = 1 \cdots 4)$ are chosen such that the resistance and its first derivative remain continuous at the transition frequencies ω_{c1}, ω_{c2} and ω_{g1}, ω_{g2}, respectively. They denote the following terms (the coefficients $a_i^{(g)}$ are obtained simply replacing the index (c) by the index (g) and using γ_g instead of γ_c):

$$\begin{aligned}
a_4^{(c)} &= \frac{\gamma_c \cdot \nu_c + \frac{1}{4} \cdot \left(\frac{1}{2} - \nu_c\right) \cdot (4 - \nu_c[1 - \gamma_c^2])}{4 - \nu_c - \frac{1}{4} \cdot \left(\frac{1}{2} - \nu_c\right) \cdot (4 - \nu_c[1 - \gamma_c^2])} \\
a_3^{(c)} &= \frac{1}{4} \cdot \left(\frac{1}{2} - \nu_c\right) \cdot (1 + a_4^{(c)}) \\
a_2^{(c)} &= \frac{1}{\gamma_c} \cdot (a_4^{(c)} - a_3^{(c)}) \\
a_1^{(c)} &= a_2^{(c)} + \gamma_c \cdot a_3^{(c)}
\end{aligned} \tag{21}$$

where

$$\gamma_c = \left(\frac{\omega_{c1}}{\omega_{c2}}\right)^2 = \left[\frac{wt}{\sqrt{2}(w+t)^2}\right]^2$$

and

$$\gamma_g = \left(\frac{\omega_{g1}}{\omega_{g2}}\right)^2 = \left[\frac{w_g t}{(2w_g + t)^2}\right]^2.$$

A.6 The Coefficients $a_i^{(L)}$

Corresponding to the terms $a_i^{(c)}$ presented above the coefficients $a_i^{(L)}$ $(i = 0 \cdots 5)$ cause smoothing of the inductance curve. They represent the following expressions:

$$\begin{aligned}
a_3^{(L)} &= \frac{(\nu_{z2} - \nu_{z1})(1 + \eta_1)(1 - \eta_4) + 4\eta_2 + \eta_4(1 - 3\eta_1)}{(\nu_{z1} - \nu_{z2})(1 + \eta_1)(1 - \eta_3) + 4 - \eta_3(1 - 3\eta_1)} \\
a_2^{(L)} &= \frac{1}{1 + \eta_1} \cdot [a_3^{(L)}(1 - \eta_3) - \eta_2 - \eta_4] \\
a_4^{(L)} &= -\frac{9}{2}\frac{w}{t} \cdot (\eta_4 + a_3^{(L)} \cdot \eta_3) \\
a_5^{(L)} &= \left(\frac{2}{9}\frac{t}{w}\right)^2 \cdot a_3^{(L)} + a_4^{(L)} \\
a_1^{(L)} &= \frac{\nu_{z1}}{4 - \nu_{z1}} + \eta_2 \cdot a_2^{(L)} \\
a_0^{(L)} &= \left(1 - \frac{L_{e\infty}}{L_{\mathrm{DC0}}}\right) \cdot \left[a_1^{(L)} + \left(\frac{w}{w_g}\right)^2 \cdot a_2^{(L)}\right]
\end{aligned} \tag{22}$$

$$F_L^{(c)} = \begin{cases}
\frac{p_{c0}}{s} \cdot \left\{ \frac{1}{a+b} \cdot \left[\pi b + b \cdot \ln\left(\frac{8\pi a}{a+b}\right) - (b-a) \cdot \ln\left(\frac{b-a}{b+a}\right) - b \cdot \ln\frac{2t_H}{s} \right] \right. \\
\quad + \frac{t_H}{s} \cdot \left[p_{c1}p_{c3} - p_{c2} - \frac{b}{a}p_{c4} + p_{c5} + (p_{c2} - p_{c3} + \frac{b}{a} - 1 - p_{c5}) \cdot \ln\frac{2t_H}{s} \right] \\
\quad + \left(\frac{t_H}{s}\right)^2 \cdot \left[p_{c3}\left(1 - \frac{3}{2}p_{c1}\right) + \frac{3}{2}p_{c1} - 2p_{c2} + 1 + \frac{3}{2}\frac{b}{a}p_{c4} - \frac{b}{a}\frac{b-a}{b+a} \right. \\
\quad \left. \left. \left. + \left(2p_{c2} + p_{c1}(p_{c3} - 1) - \frac{b}{a}p_{c4}\right) \cdot \ln\frac{2t_H}{s} \right] \right\} \\
\qquad \text{for } t_H \le \frac{s}{2} \\
\frac{1}{2s} + \frac{t_H}{s^2} + \frac{p_{c0}}{s} \cdot \left\{ \frac{\pi b}{a+b} + \frac{1}{2}p_{c6} + \frac{1}{8}\left[-p_{c1} + p_{c3}(p_{c1} + 2) - \frac{b}{a}p_{c4} - 2\frac{a^2 + b^2}{a(a+b)} \right] \right\} \\
\qquad \text{otherwise}
\end{cases} \tag{17}$$

$$F_L^{(g)} = \begin{cases}
\frac{p_{c0}}{s} \cdot \left\{ \frac{1}{a+b} \cdot \left[\pi a + a \cdot \ln\left(\frac{8\pi b}{b-a}\right) + b \cdot \ln\left(\frac{b-a}{b+a}\right) - a \cdot \ln\frac{2t_H}{s} \right] \right. \\
\quad + \frac{t_H}{s} \cdot \left[\frac{a}{b}p_{c1}p_{c3} + \left(1 - \frac{a}{b}\right)p_{c1} - p_{c2} - p_{c4} - p_{c5} + \left(-\frac{a}{b}p_{c3} + p_{c2} + \frac{a}{b} - 1 + p_{c5}\right) \cdot \ln\frac{2t_H}{s} \right] \\
\quad + \left(\frac{t_H}{s}\right)^2 \cdot \left[\frac{a}{b}p_{c3}\left(1 - \frac{3}{2}p_{c1}\right) + \frac{3}{2}\frac{a}{b}p_{c1} - 2p_{c2} + 2 - \frac{a}{b} + \frac{3}{2}p_{c4} - \frac{b-a}{b+a} \right. \\
\quad \left. \left. \left. + \left(2p_{c2} + \frac{a}{b}p_{c1}(p_{c3} - 1) - p_{c4}\right) \cdot \ln\frac{2t_H}{s} \right] \right\} \\
\qquad \text{for } t_H \le \frac{s}{2} \\
\frac{1}{2s} + \frac{t_H}{s^2} + \frac{p_{c0}}{s} \cdot \left\{ \frac{\pi a}{a+b} - \frac{1}{2}p_{c6} + \frac{1}{8}\left[-\frac{a}{b}p_{c1} + \frac{a}{b}p_{c3}(p_{c1} + 2) - p_{c4} - 2\frac{a^2 + b^2}{b(a+b)} \right] \right\} \\
\qquad \text{otherwise}
\end{cases} \tag{18}$$

---

with

$$\eta_1 = \left(\frac{w}{w_g}\right)^4 \cdot \frac{\nu_{z1}}{4-\nu_{z1}}$$

$$\eta_2 = \left(\frac{w}{w_g}\right)^2 \cdot \frac{\nu_{z1}}{4-\nu_{z1}}$$

$$\eta_3 = \left(\frac{2t}{9w}\right)^3 \cdot \frac{\nu_{z2}-\frac{1}{2}}{\nu_{z2}+\frac{5}{2}}$$

$$\eta_4 = \left(\frac{2t}{9w}\right) \cdot \frac{\nu_{z2}+\frac{1}{2}}{\nu_{z2}+\frac{5}{2}}$$

ACKNOWLEDGMENT

The author is grateful to Prof. H. L. Hartnagel for his support and encouragement.

[1] M. Muraguchi, T. Hirota, A. Minakawa, K. Ohwada, and T. Sugeta, "Uniplanar MMIC's and their applications," *IEEE Trans. Microwave Theory Tech.*, vol. 36, pp. 1896–1901, Dec. 1988.

[2] W. Schroeder and I. Wolff, "Full-wave loss analysis of normal and superconducting transmission lines by hybrid-mode boundary integral equation method," in *1991 IEEE MTT-S Int. Microwave Symp. Dig.*, vol. I, pp. 341–344.

[3] W. Heinrich, "Full-wave analysis of conductor losses on MMIC transmission lines," *IEEE Trans. Microwave Theory Tech.*, vol. 38, pp. 1468–1472, Oct. 1990.

[4] {—}, "The influence of metallization thickness on the propagation characteristics of MMIC transmission lines," in *Proc. 1990 MIOP Conf.*, Stuttgart, pp. 182–187.

[5] P. Waldow and I. Wolff, "The skin-effect at high frequencies," *IEEE Trans. Microwave Theory Tech.*, vol. MTT-33, pp. 1076–1082, Oct. 1985.

[6] G. I. Costache, "Finite-element method applied to skin-effect problems in strip transmission lines," *IEEE Trans. Microwave Theory Tech.*, vol. MTT-35, pp. 1009-1013, Nov. 1987.

[7] R. Faraji-Dana and Y. L. Chow, "The current distribution and ac resistance of a microstrip structure," *IEEE Trans. Microwave Theory Tech.*, vol. 38, pp. 1268–1277, Sept. 1990.

[8] R. B. Marks and D. F. Williams, "Characteristic impedance determination using propagation constant measurement," *IEEE Microwave Guided Wave Lett.*, vol. 1, pp. 141–143, June 1991.

[9] W. Heinrich, "Conductor loss on transmission lines in monolithic microwave and millimeter-wave integrated circuits," *Int. J. Microwave and Millimeter-Wave Computer-Aided Engineering*, vol. 2, no. 3, pp. 155–167, 1992.

[10] H. A. Wheeler, "Formulas for the skin effect," *Proc. IRE*, vol. 30, pp. 412–424, 1942.

[11] C. P. Wen, "Coplanar waveguide: a surface strip transmission line suitable for nonreciprocal gyromagnetic device applications," *IEEE Trans. Microwave Theory Tech.*, vol. MTT-17, pp. 1087–1090, Dec. 1969.

[12] G. H. Owyang and T. T. Wu, "The approximate parameters of slot lines and their complement," *IRE Trans. Antennas Propagat.*, pp. 49–55, June 1958.

[13] G. Ghione and U. Naldi, "Coplanar waveguides for MMIC applications: Effect of upper shielding, conductor backing, finite-extent ground planes, and line-to-line coupling," *IEEE Trans. Microwave Theory Tech.*, vol. MTT-35, pp. 260–267, March 1987.

[14] H. Y. Lee and T. Itoh, "Phenomenological loss equivalence method for planar quasi-TEM transmission line with a thin normal conductor or superconductor," *IEEE Trans. Microwave Theory Tech.*, vol. 37, pp. 1904–1909, Dec. 1989.

[15] M. J. Tsuk and J. A. Kong, "A hybrid method for the calculation of the resistance and inductance of transmission lines with arbitrary cross sections," *IEEE Trans. Microwave Theory Tech.*, vol. 39, pp. 1338–1347, Aug. 1991.

[16] W. Heinrich, "Modelling of MMIC coplanar transmission lines by closed-form approximations," submitted to *Electron. Lett.*, 1992.

[17] M. Abramowitz and I. A. Stegun, *Handbook of Mathematical Functions*. New York: Dover, 1965, pp. 587–626.

[18] I. S. Gradshteyn and I. M. Ryzhik, *Table of Integrals, Series and Products*, 4th ed. New York and London: Academic, 1965, pp. 904–909.

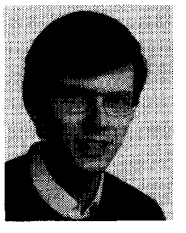

Wolfgang Heinrich was born in Frankfurt, Germany, in 1958. He received the Dipl.-Ing. and Dr.-Ing. degrees in 1982 and 1987, respectively, both from the Technical University of Darmstadt, Germany.

In 1983, he joined the staff of the Institut für Hochfrequenztechnik of the same university, where he is currently engaged in field-theoretical work on planar transmission lines.